UMass MinuteWind

Faculty and Staff Advisors:
Matthew Lackner – Mechanical Engineering – lackner@ecs.umass.edu
Richard Winn – Mechanical Engineering – winn@ecs.umass.edu

Leadership team:
Ross Adams – Chief Executive Officer
James Bedell – Chief Technical Officer
Matthew Short – Chief Information Officer

Mechanical Team:

Jonathan Cohen

Jonathan Crimble

Jack Haskell

Gabriel Sylvester

Romir Vyas

Aerodynamic Analysis Team:

Kevin Chui

Stephan Fink

Arman Paydarfar

Electrical Team:

Yonaton Kaufman – Electrical Team Leader

Jordan Chapman

Michael Horner

Joe Murphy

Brian Thompson

Nicolas Uvanovic

I. Executive Summary

The UMass Amherst Collegiate Wind Competition Team, aptly named UMass MinuteWind, is a strong team of innovative engineers with passion for design, production, and performance. The 2017 Collegiate Wind Competition (CWC) provided the MinuteWind students with an opportunity to learn about and contribute to the nation's transformation towards renewable energy through hands-on design and production of a high-performance wind turbine. The MinuteWind 2017 leadership identified areas for improvement from the 2016 test turbine design, and strategically allocated team effort to conduct research and development towards an improved design. The introduction of improved file management software and the assignment of proper leadership roles allowed the team to operate efficiently, tracking all design changes and distributing responsibilities. These improvements have resulted in a substantially improved and thoroughly tested 2017 turbine, ready for presentation and competition.

In the 2016 CWC, the UMass Amherst MinuteWind team conceptualized, designed, and analyzed a unique and compelling product to revolutionize water decontamination and desalination. The product, the Oasis, was a wind turbine equipped with a water purification unit designed to provide clean and plentiful drinking water in areas affected by natural disasters as well as refugee camps (Figure 1, left). The Oasis was designed to be easily deployable to target areas within two weeks of the event, and the installation process was optimized to be completed within twelve hours. The proposed turbine powered a reverse-osmosis water purification unit that was capable of sustainably providing communities with water in considerable excess of the United Nations' standards on water supply. While the 2016 team experienced many successes, including winning the "Best Technical Design" award, there were obvious areas for improvement as well, especially with respect to the team's wind tunnel testing performance. As a result, the 2017 team set out to build upon the foundation laid by the 2016 team, but also strove to *innovate and adapt the turbine design and fabrication* in order to excel in the 2017 competition.

The UMass MinuteWind Team was structured with a leadership team with distinct responsibilities, and three technical teams with domain expertise. This organizational structure provided a vibrant learning experience for the students and enabled efficient and well-integrated design, fabrication, and testing of the wind turbine. The faculty advisor, Professor Matthew Lackner of the Mechanical Engineering Department, oversaw the activities of the class and provided insight when necessary. The intent of the course, however, was for the students to guide the development of the project; therefore, three leadership roles were established to monitor team progress and oversee project completion. The responsibilities of the Chief Executive Officer, Ross Adams, included organizing the team into subgroups with particular foci, overseeing all aspects of the project, and holding the parallel activities in the project to a timeline. The Chief Technical Officer, James Bedell, focused on managing the completion of the turbine assembly by finalizing design and manufacturing. The Chief Information Officer, Matthew Short, served as the engineering lead; he scheduled testing times, kept track of day by day development, and managed the acquisition and processing of wind tunnel test data. Three research and development teams were formed based on the

Figure 1: 2016 Turbine (Left) and 2017 Turbine (Right)

major components of the turbine system: 1) Mechanical Systems, 2) Aerodynamic Design and Analysis, and 3) Electrical and Controls Systems. These teams' responsibilities were delegated to meet the fundamental requirements of the turbine and competition, though the students also allocated effort dynamically to adapt to evolving needs of the project.

The 2017 CWC experience introduced MinuteWind students to alternative solutions for energy generation and also highlighted the importance of innovation and teamwork. The 2017 turbine design came with several technical challenges that *highlighted the complexities of wind power generation, and created opportunities to develop innovative solutions*. The first step towards the development of the 2017 turbine was the identification of areas of improvement in the 2016 design, as well as integrating a new tower assembly capable of yawing. To attack these design objectives, the team leaders applied a parallel design method by strategically dividing interdependent tasks among the separate teams. The intention of this approach was to minimize downtime by prioritizing the tasks that were required for finalization of other tasks. The parallel design method resulted in the simultaneous completion of a new hub-rotor assembly and yaw system. These components allowed for wind tunnel testing in the early stages of the design process, which enabled refinement and optimization of the rotor design and controller.

The resulting wind turbine (Figure 1, right) produced by the 2017 UMass Amherst MinuteWind team (Figure 2) is a substantially improved version that has been *designed, optimized, and tested for all aspects of the competition*. This report details the design process, fabrication methods, and testing procedures for the turbine, including preliminary wind tunnel results that have been utilized to optimize the mechanical and electrical system designs. UMass MinuteWind is confident in presenting the 2017 turbine design, with innovative design features and improvements from the previous competition.

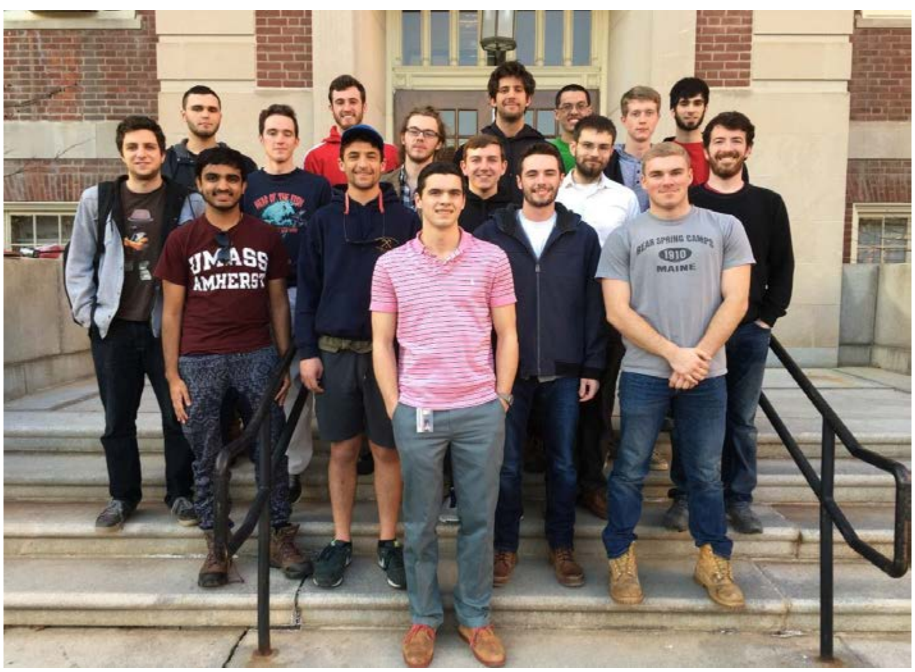

Figure 2: 2017 UMass Amherst MinuteWind Team

UMass MinuteWind not only focused on the competition, but also intended to prepare the students for professional careers by honing individual skillsets and offering team collaboration and outreach opportunities. After investigation of Product Data Management (PDM) software, GrabCAD

Workbench became the chosen PDM software and served as a local access point for the project. It also offered other engineering features such as tracking file versions, 3D quick view, and built in collaboration tools. This software enhanced the sophistication of the project and created a more unified team setting in which members contributed more professional material. During the semester, many members of the team spent significant time modelling parts in SolidWorks, the chosen 3D design platform, and thus developed proficiency with the software. Considering this growth, an external goal was established to have proficient team members take the Certified SolidWorks Associates (CSWA) Exam after the competition for resume enhancement. Furthermore, the CWC experience offered team members an opportunity to make positive societal impacts, by contributing to a "Girl Scout Day" hosted by the College of Engineering at UMass on April 8th, 2017. At the event, the MinuteWind team will discuss wind energy and present their test turbine to a troupe of 50 elementary and middle school girl scouts. Overall, each member of the team has gained an invaluable experience that prepares them to enter a professional work environment and to make positive contributions to society.

II. Design Objective

The UMass MinuteWind 2017 team systematically designed, tested, and optimized a high-performance wind turbine that operates efficiently and robustly in all facets of the 2017 Collegiate Wind Competition (CWC). The *overall objectives* for the 2017 team were (I) to improve upon the 2016 turbine performance and (II) to adapt the design to account for the new competition requirements. The UMass MinuteWind 2017 team analyzed the 2016 team's design and performance, as well as the new competition requirements, and identified areas of improvement and strategies for maximizing turbine performance. To accomplish the overall objectives, the team identified the following *critical design objectives*:

1. Improve the mechanical design and fabrication of the hub system, to enable vibration-free rotation and efficient transmission of torque from the rotor to the generator.
2. Assess different aerodynamic rotor designs, specifically by varying the design tip speed ratio, to maximize below rated power production
3. Adapt the electrical system architecture to operate robustly in all conditions, with an emphasis on performance in low wind speeds and consistent powering of the microcontroller.
4. Design and fabricate a yaw system that can dynamically respond to changing wind conditions and keep the rotor orientation upwind with minimal change in yaw angle.
5. Utilize wind tunnel testing to enable refinement and optimization of the aerodynamic and electrical control designs.

The remainder of the report details the technical design of the turbine, with a particular focus on the methods used and insights gained to satisfy the five design objectives just listed. The resulting final turbine design is a product of many rounds of design iterations based on empirical evidence derived from analysis and experimentation.

III. Technical Specifications

III.1 – Wind Turbine Overview and Components

The UMass Amherst MinuteWind wind turbine is a 3-bladed, upwind, horizontal axis wind turbine with a 45-cm rotor diameter, passive yaw system, and actively controlled electrical system with a permanent magnet generator. Figure 3 shows a model of the turbine and identifies the major components. The wind turbine has 3D printed blades attached to a 3D printed hub to form the rotor. The rotor efficiently produces power in below-rated conditions by using low Reynolds numbers airfoils (S834) and optimized chord and twist distributions determined with an in-house Blade-Element Momentum (BEM) aerodynamic analysis code. The rotor was modeled in SolidWorks and then manufactured with a Stratasys Eden 3D printer. This technique enabled the production of optimal rotor topologies, as well as rapid prototyping for testing of various design iterations.

The mechanical coupling of the rotor to the electrical generator was implemented using a modified machining collet. The generator is mounted on the front of an aluminum bracket while the rear of the bracket is connected to the tail vane. The turbine nacelle is mounted on an integrated passive yaw system made using an aluminum baseplate with two pressed brass bushings, and a thrust bearing supported by a locking collar. The bushings and thrust bearing allow for low friction rotation of the turbine while it snuggly fits to the steel tower shaft. The tower is hollow to allow for electrical connection between the generator and the external circuit. The baseplate was designed for compatibility with the base flange bolt pattern in the competition wind tunnel. The tower, rotor, and other critical components were tested via Finite Element Analysis to confirm the robustness of the model, and to ensure the safety of the users.

ITEM NO.	PART NUMBER	QTY.
1	Wind Tunnel Baseplate	1
2	Auxiliary Baseplate	1
3	Baseplate Tower Mount	1
4	Tower Shaft	1
5	Yawing Sleeve	1
6	Set Screw Shaft Collar	1
7	Thrust Needle Nose Bearing	1
8	Oil Embedded Thrust Bearing	2
9	L Bracket	1
10	Tail Vane Bracket	1
11	Rotor Hub	1
12	Blade Root Key Piece	3
13	Optimal Blades	3
14	Rotor Nose Cone	1
15	Tail Vane	1
16	60 W, 3000 rpm DC Motor	1

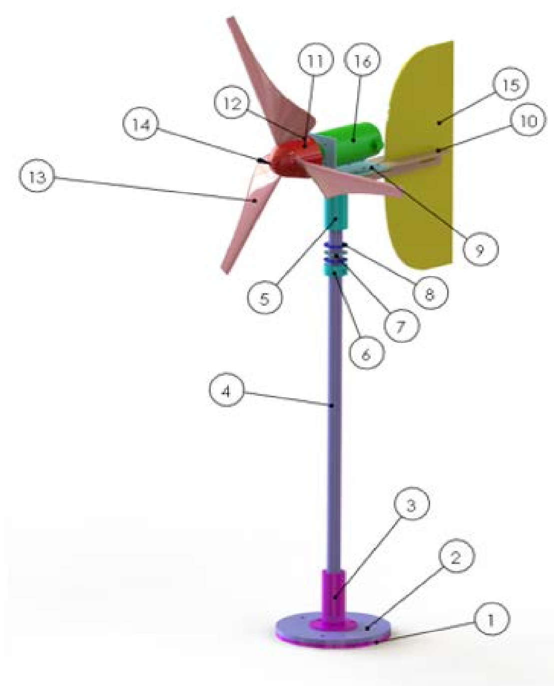

Figure 3: 2017 Turbine Model and Bill of Materials

The electrical and control system has been optimized experimentally to yield maximum power output in below-rated wind conditions as well as control of the rotor power and speed during above rated or safety shut-down conditions. A 12-V, permanent magnet DC motor was chosen for a generator as it was compatible with the expected RPMs and turbine requirements. A microprocessor was used to implement the primary feedback control system, gathering real time information on rotor speed and power output and then adjusting the system accordingly to obtain the desired output. The microprocessor can also force regenerative braking to control rotor speed during high wind speeds.

III.2 – Mechanical Improvements to the Turbine Design

The 2016 turbine had deficiencies that were addressed in the 2017 turbine design. The most significant design change involved the attachment of the blades to the hub, and the hub to the generator. In the 2016 design, a blade was printed as one piece with 1/3rd of the hub. The rotor was then assembled by screwing the three blade-hub sections to a circular aluminum subsection (Figure 4). This final assembly was attached to the generator shaft via a set screw. There were numerous problems with this design, including: imprecise attachment of blade/hub sections to the aluminum hub subsection, a poorly machined aluminum hub subsection, and improper alignment of the hub assembly with the center axis of the generator shaft. All of the aforementioned design flaws contributed to unbalanced rotation of the hub assembly, and caused the turbine to violently shake when testing at any wind speed.

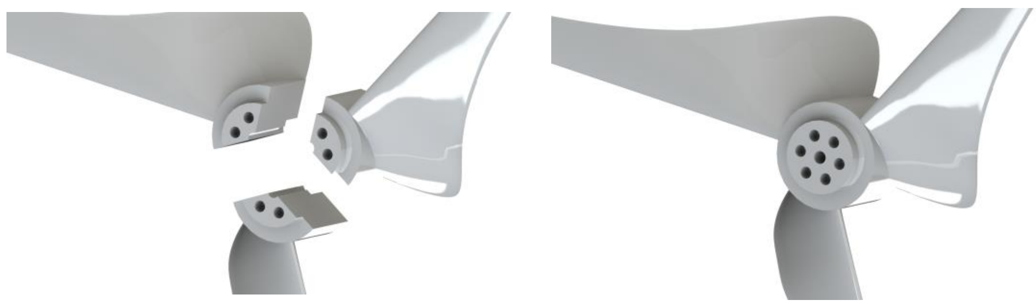

Figure 4: 2016 Hub-Rotor Assembly

The hub assembly was redesigned for the 2017 turbine to achieve balanced rotation and improved transmission of rotor torque to the generator shaft. The hub/blade sections were replaced by separately printed blades and a universal hub, shown in Figure 5. The redesign featured blades printed with a slotted key that slides into a keyway in the hub. The center of the hub was threaded to attach the assembly to the generator, as shown if Figure 6. The set screw attachment was replaced by modifying a standard 0.25” machining collet. The tool end of the machining collet tightens onto the generator shaft, and the 0.5” shaft of the collet was threaded for hub installation. A nose cone with a helicoil acted as a tightening nut for the finalized assembly as seen in Figure 6. The results of this redesign eliminated all shaking and vibration, and increased the turbine efficiency, performance, and longevity.

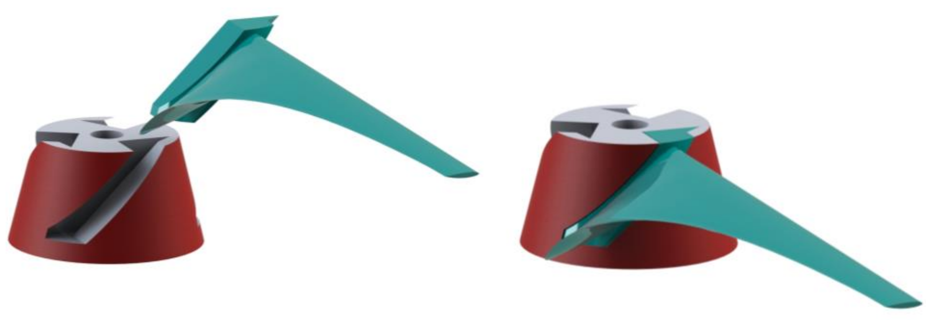

Figure 5: 2017 Hub-Rotor Assembly

Additional design changes involved the tower shaft and the routing of the electrical wires. In the previous design, the tower shaft had welded brackets on either end. The joints were not precisely at a 90 degree angle, and prevented the turbine rotor plane from being oriented orthogonally to the oncoming wind. Additionally, the pervious tower design did not house the electrical wires inside of the tower shaft. These problems were averted by machining new top and bottom baseplates. The top baseplate was designed for use with the yaw bearing. The bottom baseplate mimics the top baseplate design. A second set screw was added to secure the baseplate to the tower shaft. The final tower assembly stands vertically and has over 0.5" internal diameter to route the electrical wires.

ITEM NO.	PART NUMBER
1	S834 Nosecone
2	S834 Hub
3	Modified Machine Collet
4	Half Inch Collet Insert
5	Locking Nut
6	Compact DC Motor

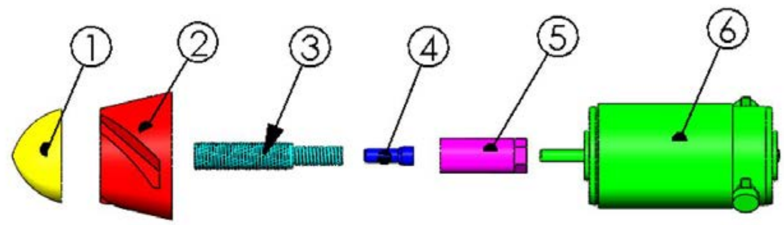

Figure 6: Hub Assembly

Many new components were manufactured for the final assembly of the 2017 turbine including the baseplate, base mounting bracket, tower shaft, yawing bracket, motor mounting bracket, tail vane assembly, and the modified machining collet, seen in Appendices B-H. Other than the steel tower shaft and modified collet, all other components were manufactured from aluminum. A lathe, milling machine, bandsaw, and belt sander were the primary tools used in the manufacturing process.

The yawing bracket and modified machining collet were the most challenging components to manufacture. The yawing bracket, shown in Appendix C, included installation of press fit brass bushings that required boring of the inner diameter of the yawing bracket on either side. The final diameter of the bored hole was only a few thousandths of an inch larger than the bushing outer diameter. This tolerance provided a secure press fit. The modified machining collet required the ½" shank to be threaded and the final length to be cut down. The shank was threaded using a lathe and special cutter, and many small individual cutting passes were performed for proper threads. The remaining components required more basic machining techniques and had larger tolerances.

IV. Static Performance and Aerodynamic Analysis

IV.1 – Aerodynamic Design and Analysis

An in-house aerodynamic analysis code created in MATLAB was used to perform airfoil selection, rotor design optimization, and performance assessment. The code required an input of lift and drag coefficients versus angle of attack for a particular airfoil. The user specified several input parameters including the rotor radius, airfoil distribution, number of blades, design wind speed, and design tip-speed ratio. The code first determined an optimal chord and twist distribution using blade-

Figure 7: Rotor with S834 Airfoils and Optimized Chord and Twist Distributions

element momentum (BEM) theory (Figure 9). The rotor was then analyzed using an iterative BEM solver to find the power coefficient (*Cp*) as a function of the tip speed ratio (λ). This method was derived from the text *Wind Energy Explained*, by Manwell, McGowan and Rogers[1]. The code was validated with the NREL code *AeroDyn v14* and yielded *Cp* values within 3% at a given value of λ. The equations defining *Cp* and λ are given below.

$$C_P = \frac{P}{\frac{1}{2}\rho\pi R^2 U^3}, \qquad \lambda = \frac{\Omega R}{U}$$

A variety of airfoils that have been used for small wind turbines, or could perform well at low Reynolds numbers, were considered and analyzed including: S822, S823, S824, E387, SG6040, SG6042, SG6043, FX63137, S833, S834, and S835. The S834 airfoil, with profile shown in Figure 8, was then chosen for the final design. While the SG6040 family of airfoils yielded the highest power coefficient in the BEM code, due to fabrication limitations, the S834 airfoil was chosen for the turbine blades due to the larger thickness to chord ratio of 15%. Because of the 45-cm rotor diameter, the Reynolds number experienced by the blades is quite small, with values of approximately 20,000 depending on the spanwise position and wind speed. Thus, the coefficient of lift and drag data for a Reynolds number of 50,000 were chosen, which is the lowest value available for the S834, as shown in Figure 8.

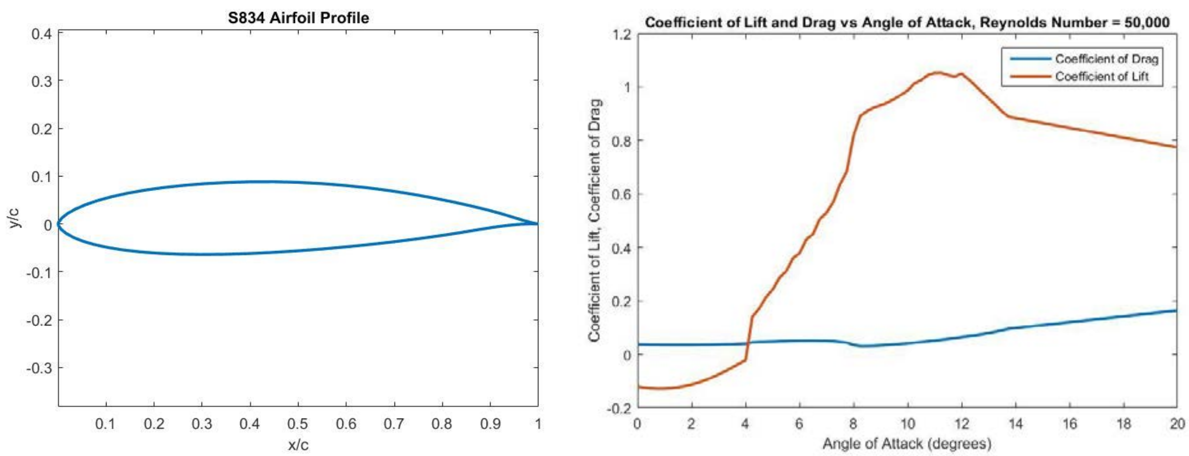

Figure 8: Profile of the S834 Airfoil (Right) and Coefficient of Lift and Drag vs. Angle of Attack (Right)

Due to the need for rapid prototyping, the turbine blades were fabricated from ABS plastic using 3D printing technology. The advantages of 3D printing include customization and ease of manufacturing, using an ideal geometry. The blades and hub were modeled in SolidWorks before being manufactured with a Stratasys Eden 3D printer.

[1]The method used was derived from *Wind Energy Explained: Second Edition*, by Manwell, McGowan and Rogers.

The turbine was modified and optimized relative to the 2016 design. The S834 airfoil was again chosen due to the balance of efficient aerodynamic performance and a thick profile (to allow ease of manufacturing and avoid issues of resolution with the 3D printer). A range of values for the design λ (4, 5, 6 and 7) were evaluated with the BEM code to balance multiple design criteria. On one hand, a higher value of design tip speed ratio resulted in a higher rotation speed for a given wind speed, and since the generator voltage was dependent on rotor speed, this was advantageous. Conversely, a lower value of design tip speed ratio resulted in blades with larger chords which were easier to manufacture (Figure 9), as well as increased rotor torque, which was beneficial for start-up of the wind turbine (Figure 10). These design considerations were evaluated by manufacturing and testing blades with design tip speed ratios of 6 and 7, and the test results are discussed in Section IX.

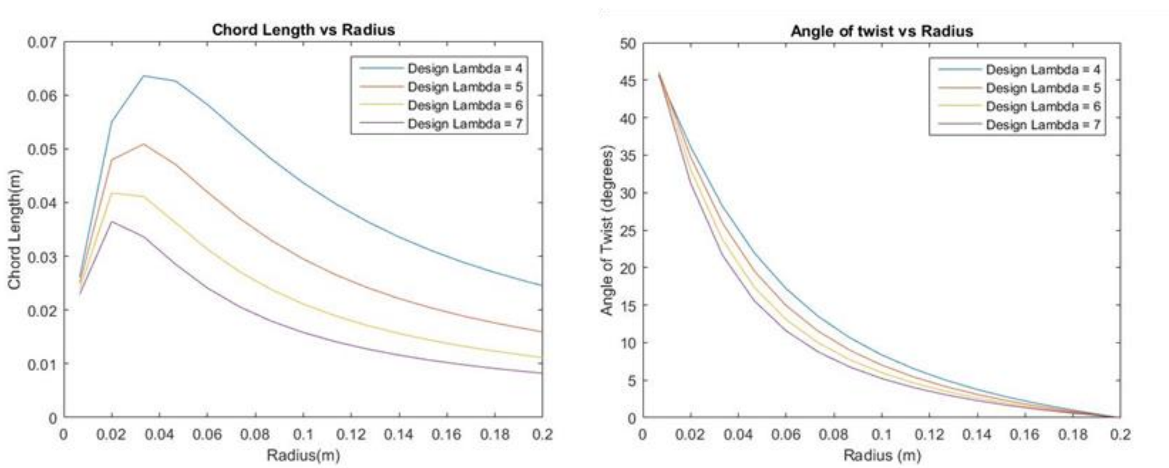

Figure 9: Chord Length vs Radius (Left) and Angle of Twist vs. Radius (Right)

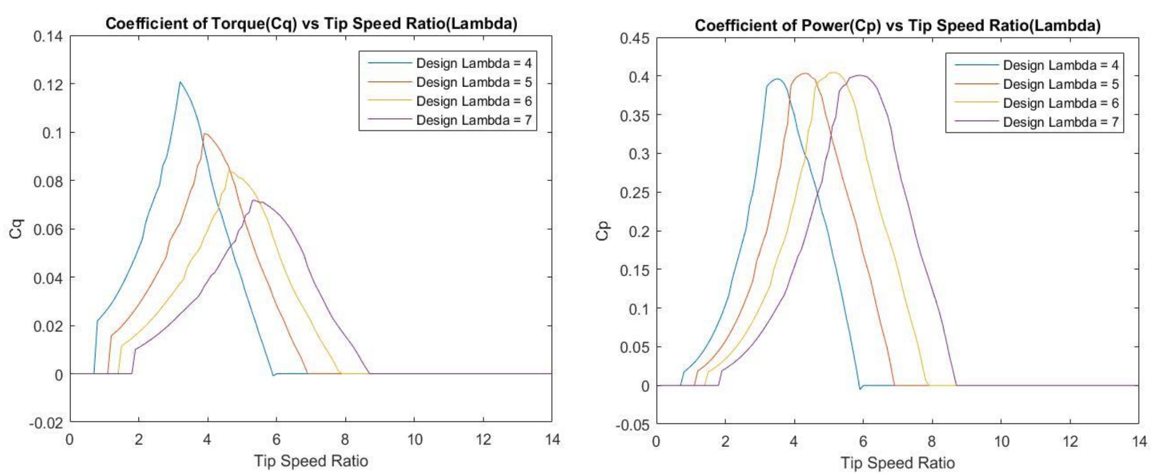

Figure 10: Cq vs Tip Speed Ratio (Left) and Cp vs Tip Speed Ratio (Right)

IV.2 – Annual Energy Production Estimates

While the 2017 team's primary focus was on the design and testing of the test turbine for the CWC wind tunnel tests, the analysis of annual energy production (AEP) has been performed for the 2016 market turbine. The 2016 market turbine was a 3.1 kW horizontal axis wind turbine with a 3.1 m rotor radius. The AEP for the market turbine was evaluated as a function of mean wind speed, with values ranging from 2 m/s to 8 m/s, and the results are shown in Figure 12. In all cases, the cut-in wind speed (3 m/s), and cut-out wind speed (20 m/s) were held constant, while the rated wind speed and the overall turbine efficiency (aerodynamic power coefficient multiplied by mechanical and electrical efficiency, i.e. *Cp*eff*) varied. The rated wind speeds analyzed were 8 m/s (solid lines), 9 m/s (dashed), and 10 m/s (dotted). The efficiency values analyzed are 0.2 (blue), 0.25 (red), and 0.3 (green). These efficiency values were based on the predicted *Cp* from the BEM code, and a reasonable estimate of mechanical and electrical efficiency. To calculate AEP, a power curve was created that was a cubic function of wind speed, scaled by the *Cp*eff* value, between cut-in and rated, and was constant between rated and cut-out (Figure 11). A Rayleigh distribution modeled the wind speed probability density function (pdf) for a given mean wind speed value, and the average power was then calculated by integrating the product of the power curve and pdf versus wind speed, between cut-in and cut-out. The average power was then multiplied by 8,766 hours to obtain AEP. The output was compared to the necessary energy input to the water treatment unit (black line in Figure 12). It was assumed that seawater was being desalinated with a specific energy of 5 kWh/m^3, and that 2,000 L were produced per day. Figure 12 demonstrates that the Oasis turbine will produce more than enough energy to meet the water production requirements, except at sites with extremely low mean wind speeds.

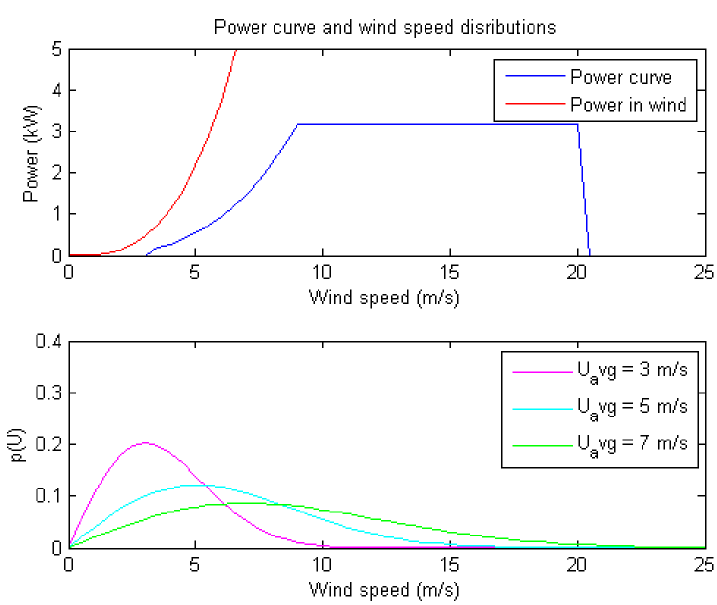

Figure 11: Market Turbine Power Curve (Top) and Wind Speed Probability (Bottom)

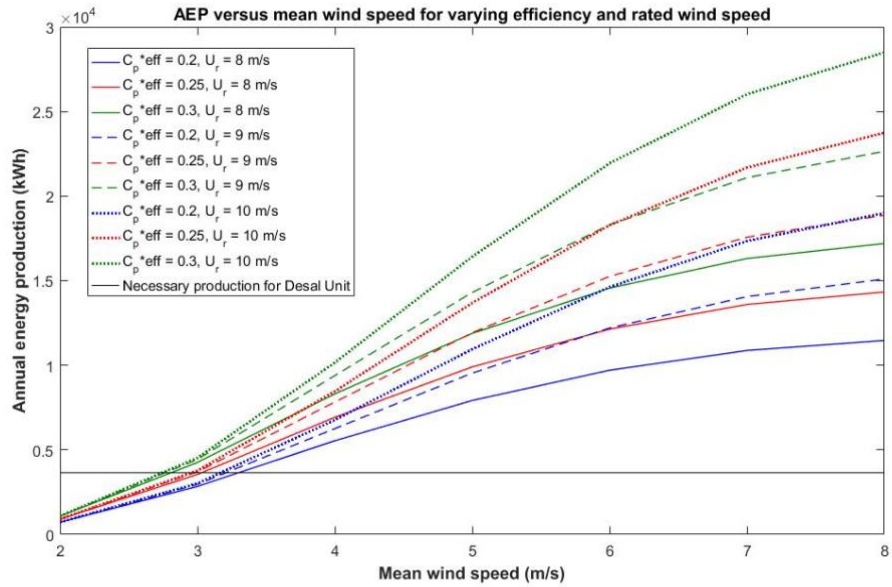

Figure 12: AEP vs. Mean Wind Speed for a Variety of Cp and Speed Values

V. Description and Analysis of the Yaw System

V.1 – Design Objective

To keep the turbine nacelle directed into the wind, a yawing system was integrated into the supporting tower. In addition to redesigning the tower assembly, inclusion of a yaw function also required the addition of a tail vane. The objective of the design was to create a reliable and robust system that allowed the turbine to rapidly adapt to changing wind conditions, considering the high speed rotational requirements that will be seen in competition. To achieve this objective, several design options were evaluated including: an internal bearing system housed within the steel tower, an external bearing system that would slide over the exterior of the tower, and an internally lubricated turntable to rotate either the whole assembly or upper assembly. After evaluating the various options, the external bearing system was chosen, using a thrust bearing as the primary means of rotation.

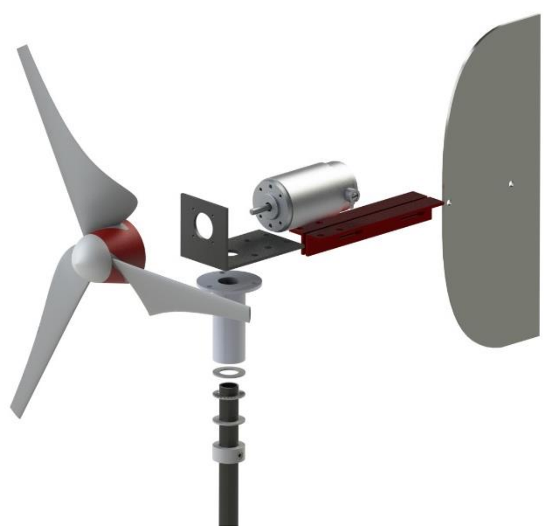

Figure 13: Upper Assembly Exploded View

The internal bearing system was ruled out due to complex installation and manufacturing methods. The bearing must be secured within the steel shaft and an intricate mounting system would be required for connection between the tower and turbine nacelle. The internally lubricated turntable was an effective solution but was found to have certain limitations. The placement of a turntable below the upper tower assembly was not geometrically possible with the stated volume constraints. The placement of a turntable at the base of the tower assembly would have higher bending stresses and would be subject to uneven loading, causing unwanted friction or possible locking of the yaw system. For these reasons both the internal bearing system and the turntable system were rejected, and the more compact thrust bearing solution was selected.

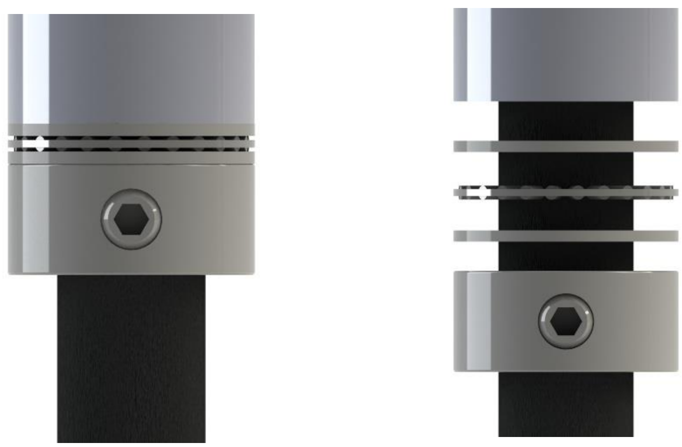

Figure 14: Thrust Bearing and Adjoining Clamping Collar

A lubricated thrust bearing and adjoining clamping collar were chosen to enable rotation of the turbine nacelle, as seen in Figure 14. This thrust bearing was chosen for many reasons including: adjustability of clamping collar, low cost, low friction, and ease of integration into existing assembly. An aluminum yawing sleeve, which rests atop the thrust bearing, was designed to adjoin the tower and the turbine nacelle. Brass bushings were press fit into the yawing sleeve to reduce rotational friction while providing a snug fit to the tower shaft. To fit within the geometric constraints, a boom and fin style vane illustrated in Figure 13, was employed. The length of the boom was chosen based from the allowable volume for the turbine. A variety of tale vane geometries were tested on the turbine. The final design was selected based on the yawing response speed and volume constraints. Preliminary testing results are discussed next, and then further presented in Section IX.

V.2 – Yaw System Testing

During trials in the wind tunnel, the yaw system performed very well. The turbine self-aligned relative to the oncoming wind when subjected to a perturbation that misaligned the rotor. Initially, the steady state yaw-angle of the turbine was approximately 10-degrees, however, with a counterclockwise rotation out of the direction of flow. It was determined that the precession of the rotor assembly was not taken into consideration during the design of the tail vane. An increase in tail fin surface area corrected this issue yielding a responsive, accurate, and reliable yawing system.

VI. Analysis of Loads and Safety Factor

VI.1 – Rotor Loads Analysis

Ensuring a high margin of safety is a vital aspect when designing the turbine to be dependable and effective. In order to verify safe operation of the turbine during testing, computational models and engineering analysis were used to evaluate the response of the turbine components to loading. Using ANSYS Workbench 2015, a tool for finite element analysis, the rotor's structural response and dynamics were modeled. The blades were printed with ABS plastic, and thus properties of the material were applied. The greatest concern for failure is the bending stresses due to thrust forces acting on the blades. Figure 15 shows the simulated results of the blades subjected to 11 m/s wind speeds. A frictionless support constraint was placed on the downwind face of the rotor. A wind load and rotational velocity corresponding to rated wind speed (when rotor thrust is maximum) were applied to the assembly. The wind load was modeled by a constant pressure over the turbine's geometry in the negative y direction, simulating the thrust forces that would result in a maximum bending moment. These results are shown below in Figure 15.

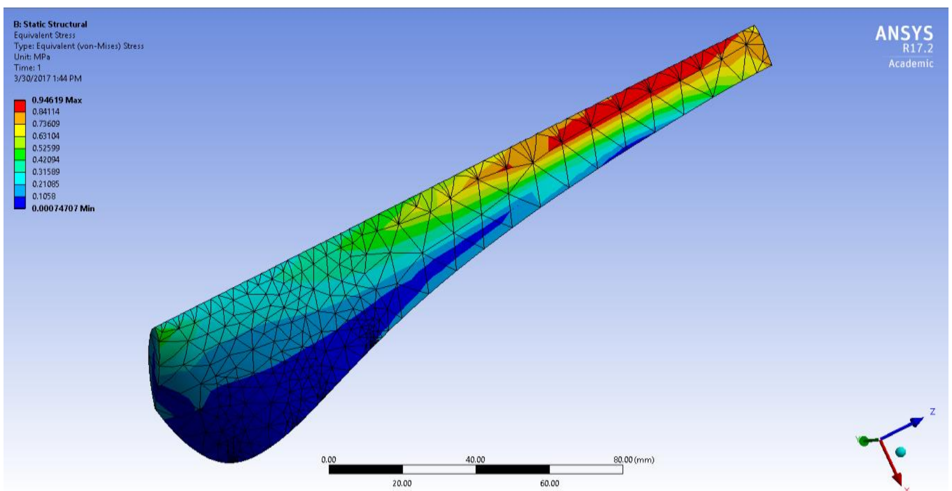

Figure 15: ANSYS Test Results on Rotor

The results of the static structural test ensured a safety factor of 51.05 times the maximum allowable yield stress of the material. The blades experienced levels of stress that fell well within the tolerable ranges of the material used. The deflection of the blades was also found to be minimal, resulting in a 0.742-millimeter maximum deflection.

VI.2 – Tower Loads Analysis

Loads on the tower were calculated based on the thrust forces acting upon the rotor at rated wind speed conditions of 11 m/s. Bending stress calculations are depicted in Figure 16. These calculations reveal a high safety factor for the tower base of 4.4 with respect to the yield strength of the tower material. The calculations were then confirmed with an ANSYS equivalent stress simulation on the tower, as seen in Figure 17. This verifies our design choices for the tower thickness and height as satisfactory.

Turbine Bending Analysis

Variables: F_t = Thrust Force
ρ = Density of Air
U = Wind Speed
R = Rotor Radius
h = height
z = Hub Height
C_t = Thrust Coeffiecient
d_0 = Outside Diameter
d_i = Inside Diameter
$\sigma_{bending}$ = Bending Stress
σ_{yield_steel} = yield stress of steel

$U := 11 \cdot \frac{m}{s}$ $\quad \rho := 1.225 \cdot \frac{kg}{m^3}$ $\quad R := 22 \cdot cm$ $\quad d_0 := 0.75 \cdot in$ $\quad d_i := 0.62 \cdot in$

$a := \frac{1}{3}$ $\quad I := \frac{d_0^{\ 4} - d_i^{\ 4}}{64}$ $\quad c := \frac{d_0}{2}$

$C_t := 4 \cdot a \cdot (1 - a) = 0.889$

$F_t := \frac{1}{2} \cdot C_t \cdot \rho \cdot \pi \cdot R^2 \cdot U^2 = 10.017\ N$ $\quad \sigma_{yield\_steel} := 250 \cdot MPa$

$z := 1.5 \cdot in$ $\quad h := 24 \cdot in + z$

$M_{base} := F_t \cdot h$

$\sigma_{bending} := \frac{M_{base} \cdot c}{I} = 56.344\ MPa$ $\quad SF := \frac{\sigma_{yield\_steel}}{\sigma_{bending}} = 4.437$

Figure 16: Turbine Tower Bending Stress Calculations

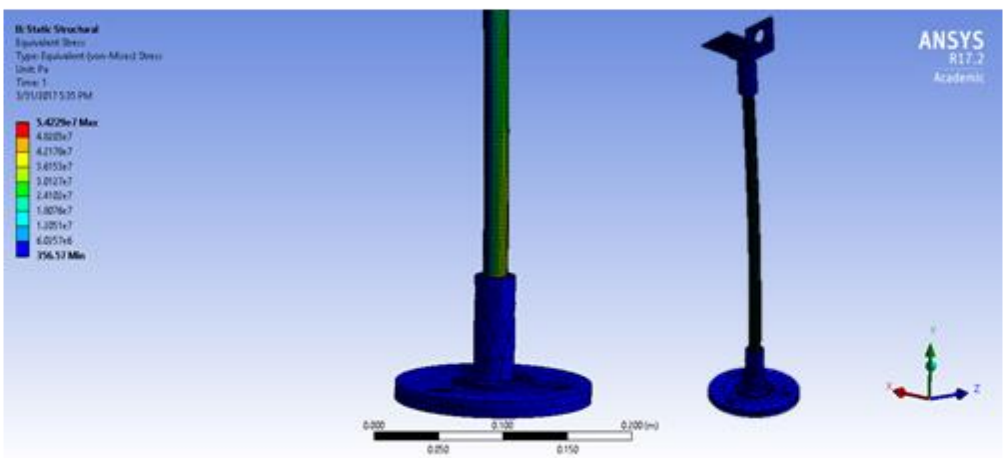

Figure 17: ANSYS Test Results on Tower

VII. Electrical System Description

In the early stages of the electrical system development, three main objectives were identified. First, the circuit must be able to control the power output and speed of the turbine at any given wind speed during various safety and shut down tasks. Next, the circuit must be capable of complete autonomous operation while at the same time powering the microcontroller. Lastly, the electrical team sought to maximize the efficiency of the circuit through minimizing electrical system losses within the circuit itself.

VII.1 – Generator and Circuit Design

The first major decision pertaining to the electrical components was choosing a motor to be used as a generator. After experimenting with motor voltages ranging from 12 to 24 V and power ratings ranging from 60 to 120 W, it was determined that the ideal motor for the test turbine would be a 12V, 60W motor. This decision was based on a number of factors: 1) the motor features a low torque constant (K_t), which enables the motor to start spinning at lower speeds; 2) complementing a low torque constant, the low initial startup torque of 21 oz.-in. allows for a lower cut-in speed for the turbine; and 3) the 60W motor is close to the maximum expected power output of approximately 30-40W based on aerodynamic analysis. Ultimately, the motor chosen features ratings of 60W, 3000 rpm, 4.9A maximum, and 68% efficiency. Figure 18 depicts the motor specifications on the left, while the torque-speed operating curve for continuous operation provided by McMaster-Carr is shown to the right.

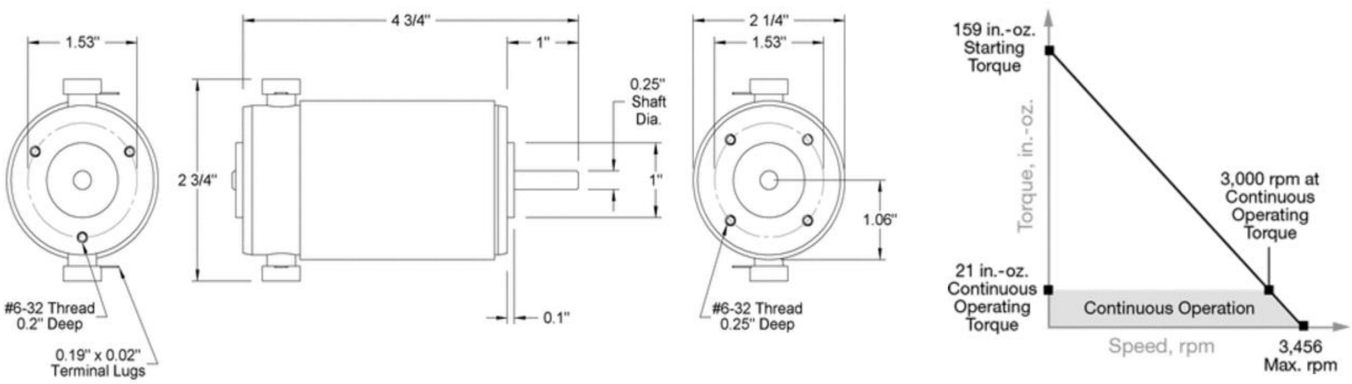

Figure 18. Motor Specifications (Left) and Continuous Operation Torque-Speed Curve Analysis (Right)

Following the generator selection, the governing circuit (Figure 19) was designed to meet the three objectives identified above. The notable components of the circuit are the inductor, load and main gate MOSFETs, Schottky Diode, voltage divider, shunt resistor, voltage regulator, mini boost circuit, SPDT-CO relay, two capacitors, and an Arduino. Each component's function and integration into the circuit are discussed below.

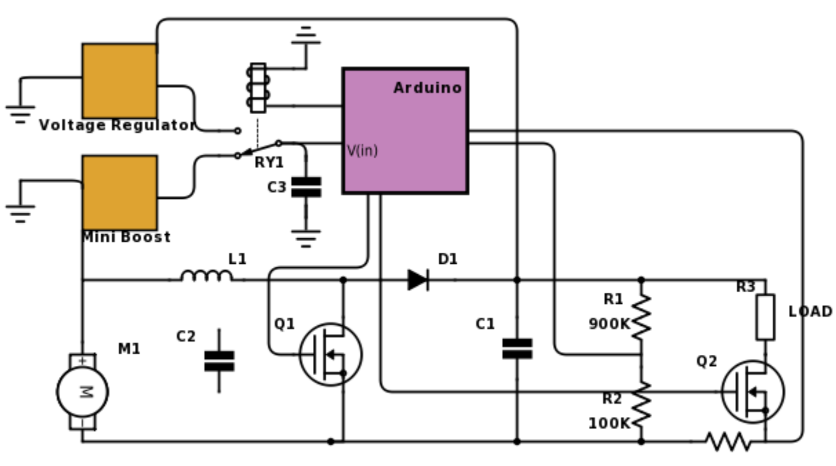

Figure 19: Circuit Diagram

The Arduino served as the microcontroller that enabled the control of the turbine (discussed below). The Arduino has a 5V operating voltage and while it can run with an input voltage between 6–20 V, it worked best in the range of 7 – 12 V. In order to operate the Arduino in low power situations, a mini boost circuit was added before the inductor. This mini boost circuit took an input voltage as low as 1.5V and boosts it to the 5V necessary to power the Arduino. Once the turbine is capable of generating 7V, the Arduino switched to being powered by the main circuit via the voltage regulator, effectively removing the mini-boost circuit out of the main circuit. To ensure a smooth transition, a capacitor was placed after the mini boost circuit to provide power to the Arduino as the switch occurs. The voltage regulator was added to ensure that when input voltages exceed 5V, the voltage was stepped down to the necessary 5V to power the Arduino.

The circuit also featured two IRF540 Power MOSFETs; these were used as switches to activate different circuit modes by controlling the flow of current throughout the circuit. Each MOSFET contained a drain, source, and gate, which were connected via the microcontroller. Through a control algorithm explained later in this report, the Arduino altered the gate value between 0 and 5 V through pulse width modulation (PWM), which allowed for control of the MOSFETs. At 0 V the gate was open, and at 5 V the gate was closed. These devices were used to expose the load and inductor at varying amounts throughout operation. Both the primary and load MOSFET were utilized to brake the turbine. While braking, the primary MOSFET was made to behave like a closed circuit, effectively shorting the leads of the generator through the inductor and primary MOSFET. The load MOSFET exposed the load after startup to ensure that the microcontroller was able to turn on before power was sent to the load, and also raised the effective resistance of the load during braking to assist in short circuiting the generator. When properly cooled, these MOSFETs can dissipate 50 Watts of power, which far exceeds the need of the load. Dissipating this much power caused the MOSFETs to heat up, so heat sinks were applied to each MOSFET in order to increase heat dissipation.

The 335 μH, 6A inductor from Pulse Electronics Corp was paired with the main MOSFET to vary the effective resistance shown to the motor. This allowed for control over RPMs as well as power output and load side voltage. As the gate voltage on the connected MOSFET increased, the MOSFET transitioned from cut-off to saturation mode. This allowed current to begin flowing through the switch, and once the gate reached 5V, the MOSFET was in full saturation, essentially acting as a short circuit. When used to brake the turbine, the MOSFET was sent into saturation and the generator was shorted across the inductor and MOSFET. This caused a dramatic increase in current, resulting in a reverse torque being applied to the generator, and thus slowing the rotation of the blades.

A Schottky diode was incorporated into the circuit to ensure that current does not flow backwards into the motor when the load voltage exceeds input voltage. The 3.3 milliFarad capacitor enabled the circuit to smooth the voltage ripple on the load side. To measure current a shunt resistor, a 0.005 Ω, 1 W device with 1% precision, was placed between the load output and ground. The voltage drop across the shunt resistor was measured and then divided by the Ohmic value of the shunt resistor, resulting in the amount of current going through the load.

The voltage divider was necessary since the Arduino can only read up to 5 volts, and the voltage across the load often exceeds that value. A voltage divider with high resistance values was placed in parallel with the load. High resistance values caused minimal loss in power through the voltage divider. A 900kΩ resistor was used in series with a 100kΩ resistor from load(+) to ground. Voltage was then measured between these resistors and multiplied by 10 to sample an accurate measurement.

VII.2 – Testing and Design Iterations

Ultimately, through multiple design iterations, the preliminary objectives for the electrical system were met, with a circuit that is more efficient and reliable than the 2016 version. Early on in the design phase, it was observed that the previous year's circuit did not contain a voltage regulator. The addition of the voltage regulator to the 2017 circuit enables safe powering of the Arduino by stepping down high voltages to a steady 5V. Additionally, the previous circuit contained two microcontrollers, one with a very low startup voltage and an Arduino. Having two microcontrollers operate the same circuit requires communication between the two which is not only difficult, but can also lead to complications during situations such as braking or emergency shutdowns. To avoid this, a single Arduino was used to control the circuit, with a mini boost circuit providing it the necessary 5V of power during low power situations such as braking.

During wind tunnel testing, a problem was identified when the circuit was not producing nearly the amount of power the aerodynamic analysis predicted. This problem was resolved by switching to a thicker gauge wire running from the generator to the circuit. This thicker wire allowed more current to pass through and resulted in a much greater power output (increasing from 3 W to nearly 20 W at the same wind speed). Lastly, because the 2016 circuit continually powered up and then shut down during CWC testing, it was determined that this was caused by a loose part since a breadboard was used for their final circuit. To prevent this problem from reoccurring, the final circuit will be soldered in an effort to increase its overall reliability.

VIII. Controls Analysis and Software Documentation

To meet the competition requirements, a control strategy was created using the Arduino and the electrical circuit. The controller was designed to optimize the power output of the turbine while still powering the microcontroller, as well as to meet the various competition performance metrics and tasks outlined by the CWC guidelines. The controller is summarized in the control states diagram (Figure 20).

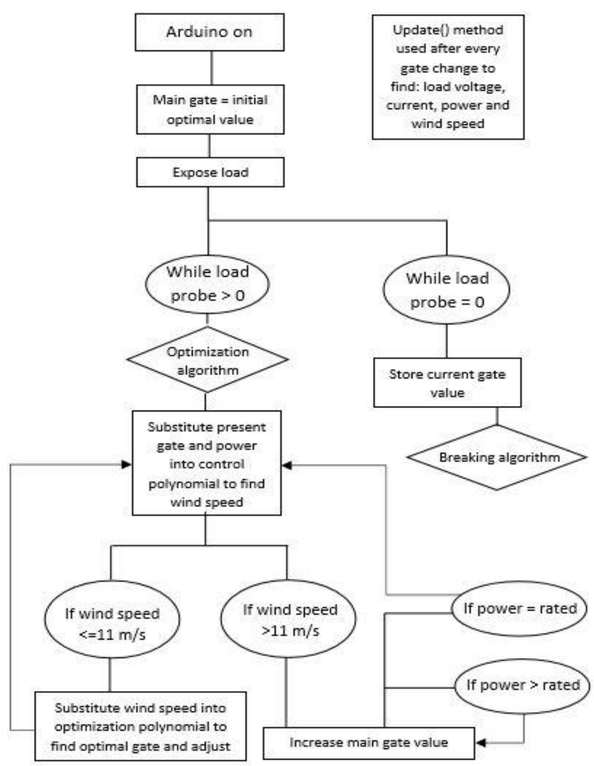

Figure 20: Controls State Diagram

VIII.1 – Startup Control

As shown in Figure 20, the controller executed different functions depending upon the operation scenario. To begin, the circuit must be in the optimal state to cut-in and send power to the Arduino without any control. This was accomplished by designing a circuit where the zero-power state of the MOSFETs required the lowest possible current from the motor and diverted no power to the load. A voltage booster was implemented to boost an input voltage range of between 2 to 5V up to 5V in order to power the Arduino at lower wind speeds. Once the Arduino received sufficient power to turn on, it raised the gate voltage of the load MOSFET, transitioning the

MOSFET from cut-off towards saturation, and beginning to send power to the load. Due to the requirements of the Arduino, some power was lost at low wind speeds as the controller could not draw enough energy to power on. The electrical team felt that the power lost at these low levels was outweighed by the utility of a larger microcontroller. Once the load voltage reached 7.5V, two relays were used to switch the power supply from a mini-boost circuit to a voltage regulator. When the switching occurred, the low voltage booster was effectively disconnected from the circuit.

VIII.2 – Below Rated and Above Rated Control

When the wind speed varies from startup to 11 m/s, the Arduino maximized the power diverted to the load while ensuring there is enough power to keep the Arduino on. By experimentally measuring the power output while increasing the inductor gate value at wind speed intervals of approximately 1 m/s, a 3D array of data was gathered that characterized power vs inductor gate value at every wind speed that was tested, depicted in Figure 21. This array of data was then analyzed in MATLAB and a surface was fit to match the data using MATLAB's linear least squares method, yielding a polynomial that best fit the data.

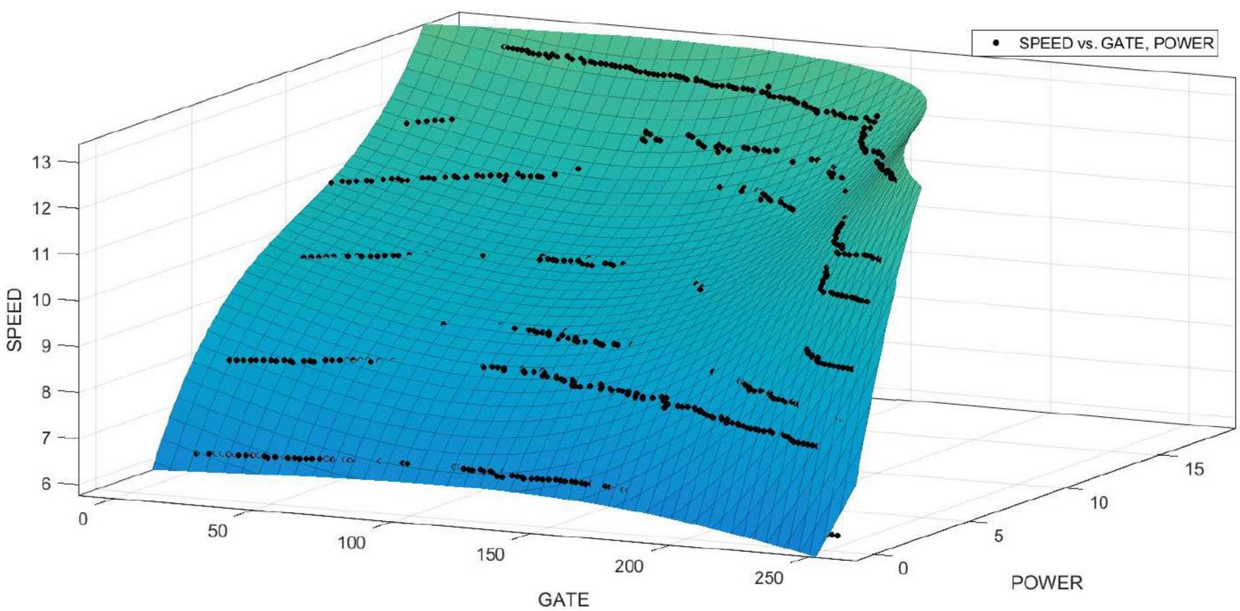

Figure 21: Gate, Wind Speed, Power Surface and Polynomial Fit

The control strategy in below rated conditions to maximize power was implemented as follows. By knowing the current state of the inductor gate as well as the power output, the wind speed can be determined using the control polynomial. The surface from the control polynomial can then be collapsed to two dimensions by finding the maximum power generated at each gate vs wind speed. Once the wind speed has been calculated from the control polynomial, it can then be substituted into a linear interpolation between the optimized gate vs wind speed points for the given wind regime to find the optimal gate value at that wind speed, seen in Figure 22.

When the wind speed exceeded the rated value of 11 m/s, the controller must maintain the speed and power output of the turbine. The rated power for the turbine was calculated through testing and programmed into the Arduino. Since the Arduino can estimate wind speed as described above, it can decide when the wind speed was above rated and increased the gate voltage of the inductor MOSFET to increase torque and slow down the turbine; inversely the gate value of the load MOSFET was reduced in order to throttle power sent to the load.

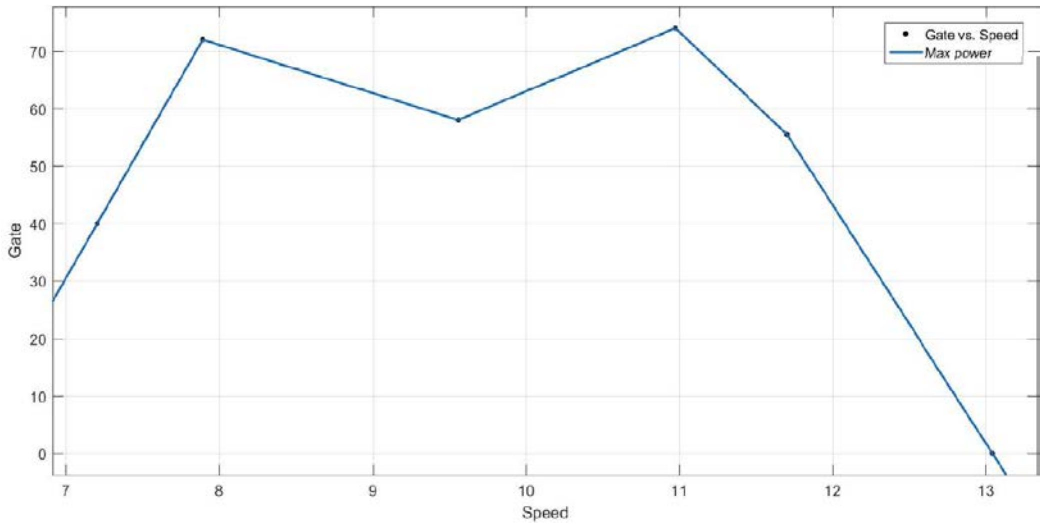

Figure 22: Optimized Gate Value vs. Wind Speed Curve

VIII.3 – Safety Shut Downs and Braking

The system maintained safety by monitoring the load as well as an emergency shutoff input. A load disconnect, or low brake signal, caused the system to run a braking algorithm. A load disconnect was detected when the system was recording wind speed and had exposed the load but detected no output current from the load using the Arduino's analog input. When braking, the controller brought the load MOSFET into cut-off (disconnecting the load) and then brought the inductor MOSFET toward saturation. This action increased the motor torque and quickly slowed the rotor.

A challenge encountered when braking was ensuring that the load side voltage did not get too high or too low. A spike in voltage could damage the microcontroller and a sharp drop would cause it to turn off and lose control. Once the load was disconnected, the resistance increased dramatically, causing any current forced through the inductor to raise the voltage much higher than if the load were connected. Careful programming was required to design a feedback loop that quickly adjusts the inductor gate voltage to maintain a safe voltage while the rotor speed decreases. Once the rotor had reached 10% of rated speed, the feedback loop adjusted the inductor gate value to maintain braking speed.

When braking at very low wind speeds, the turbine could not extract enough power at 10% of rated speed to keep the Arduino on when using just a voltage regulator. This required adding a voltage booster and relay switches to maintain power at input voltages as low as 3V. The Arduino ran a simplified feedback loop monitoring voltage and the brake signal, maintaining braking speed and minimum voltage until the brake signal was restored. At this point, the system spun back up and if the turbine produced enough voltage, the power supplies switched to the voltage regulator.

IX. Wind Tunnel Testing Procedure and Results

IX.1 – Testing environment

To optimize the test turbine performance at the CWC, UMass MinuteWind has conducted extensive wind tunnel testing using a wind tunnel located on campus. The wind tunnel has a 1 m by 1 m cross section, and is capable of producing wind speeds up to 25 m/s. The three major objectives of the tunnel testing were to: 1) integrate all components and ensure the system is operating correctly, 2) evaluate different blade designs to maximize aerodynamic efficiency, 3) test the controller under a range of testing conditions.

The team also faced challenges brought upon by the testing environment and resources. There was no direct rotor speed sensor available, and so in order to measure the RPMs of the turbine, a strobe light was used to find the frequency that seemingly froze the turbine blades. Testing the yaw system also presented a challenge, since the wind tunnel does not have a turntable similar to that in the CWC tunnel. Lacking a turntable, the turbine was outfitted with a strong, temporary tail vane that could be pushed, causing the turbine to yaw abruptly. From under the platform, a student would view the approximate angle of distortion and measure the amount of time for the turbine to return to an upwind orientation.

IX.2 – Test Results

This section presents a selection of test data obtained to date. In many cases the data was obtained with an obsolete circuit design, and thus the power output is low in some figures. Nonetheless, the testing data was invaluable for the team to better understand the system behavior and refine the controller, mechanical, and aerodynamic design. The tests were used to both characterize the behavior of the rotor and to optimize the circuit and load design. The various tests were strategically chosen to gain as much insight as possible into the turbine behavior, in the context of the competition requirements. The various tests are summarized below based on the objective of the testing procedure.

Figure 23: Wind Turbine in testing Tunnel

Testing Objective 1 – Evaluation of Rotor Design Parameters for Maximum Power

The first set of wind tunnel tests set out to determine how aerodynamic design parameters affect the experimental performance. As such, two sets of rotor blades were fabricated and evaluated, with design lambda values of 6 and 7 specified as inputs in the BEM code. The BEM code produces different optimal chord and twist distributions depending on the design lambda. Both sets of blades were tested at a range of wind speeds, which was enabled by the design of the universal hub. Figure 24 demonstrates that a design lambda of 7 is superior to 6, as power is increased by approximately 25% at U=10 m/s. It should be noted that this test was performed with a constant load and a constant gate value of zero, and before the circuit was optimized. Thus, the resulting power output is much lower than later tests. Also, between the report submission and the competition, the team plans to test a new rotor with a design lambda of 8.

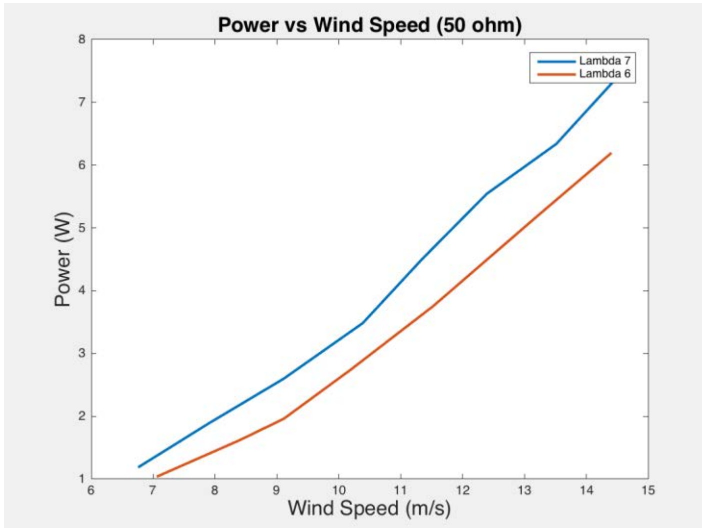

Figure 24: Power vs. Wind Speed

Testing Objective 2 – Evaluation of Electrical Load Values for Maximum Power

In order to further characterize the turbine, it was important to understand how the load resistance affected the power production. A series of tests were conducted to characterize the power production as a function of the gate values, attached to various load resistance values at a constant wind speed of 10 m/s. Figure 25 displays the test data with three different loads, through the full range of pulse width modulations (gate varies from 0 to 255). Figure 25 demonstrates that an optimal gate value exists for a given value of the load. This result provided insight into the circuit design and control algorithm, so that proper load values and gate values were chosen to maximize power output. Future tests will utilize a given load value, likely 12.5 Ω, and will refine the feedback control algorithm discussed in Section VIII.2 in order to autonomously maximize power as wind speed varies in below rated conditions.

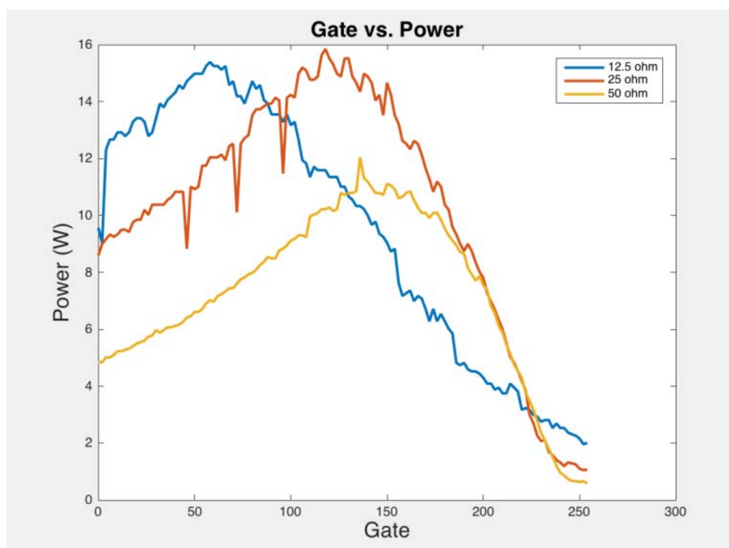

Figure 25: Gate vs. Power

Testing Objective 3 –Constant Power Control in Above Rated Wind Speeds

To address the control of rated power and speed task, the turbine was tested at higher wind speeds with the controller attempting to preserve constant power from 11m/s to 13m/s, as shown in Figure 26. The current control logic dictates that power should not increase after reaching 11m/s, which has been prioritized for now over constantly maintaining rated power. Thus, the existing code will at times decrease power more significantly than it needs to as opposed to momentarily spiking over the rated limit. Moving forward, the power curve should remain more consistent at the rated value and not contain spikes and drops. This will be addressed in future tests.

Figure 27 shows how the system regulates RPM between 11m/s and 13 m/s. As the wind speed increases, the motor is exposed to an increasing effective resistance. This increase in resistance limits the current, and therefore the power, thus creating more torque to slow down the blades.

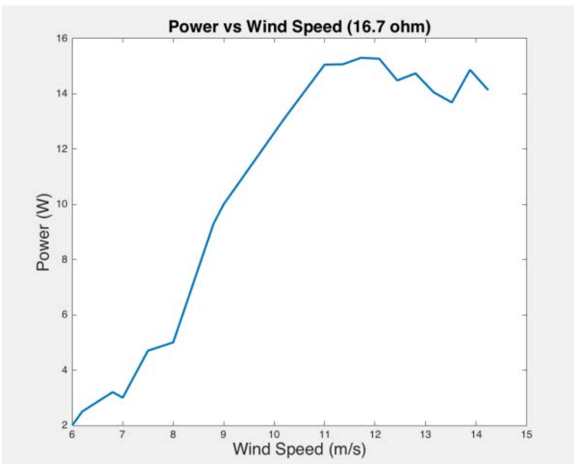

Figure 26: Power vs. Wind Speed (16.7 ohm)

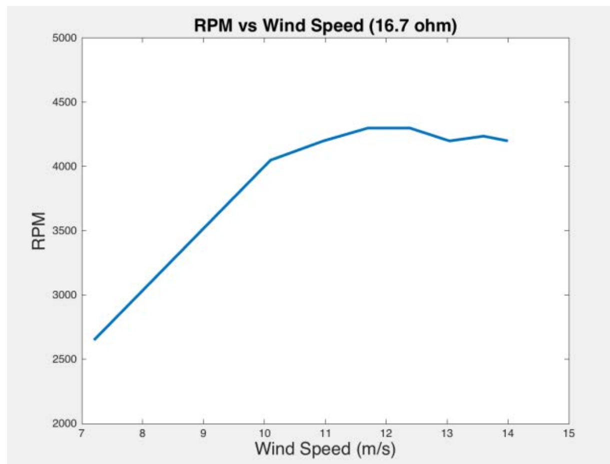

Figure 27: RPM vs. Wind Speed (16.7 ohm)

Figure 28 shows the effect of the varying gate values on power at various constant wind speeds with a constant 12.5-ohm resistance. As shown, the effect of the gate is dependent on the wind speed. At 13 m/s, the power drops continuously with increased pulse width modulation. Conversely, at rated wind speed, the gate value increases the power to a maximum before then decreasing. This data is critical to defining the control logic for the MOSFET so that it accurately controls power in above rated conditions.

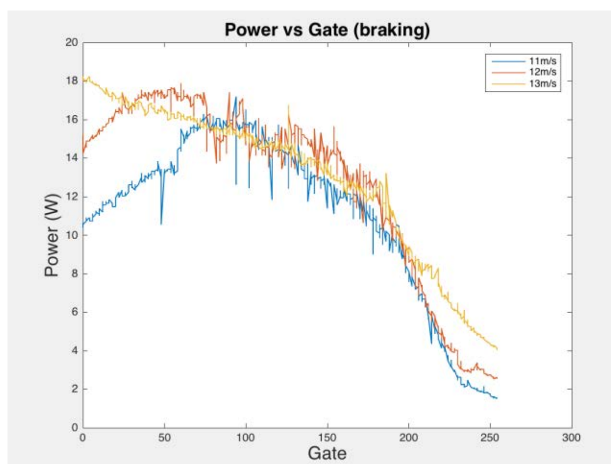

Figure 28: Power vs. Gate

Testing Objective 4 – Emergency Braking Testing

The emergency shut down tasks prompted the team to test the ability of the motor and circuit to break the turbine. Figure 29 shows how RPMs are brought to under 10% of rated in under ten seconds. Braking was initiated at t=2 and then flattens out at 10% after six seconds. This was done by drastically increasing the main gate which caused a short circuit. The blades quickly dropped in RPMs and then the gate value was slowly reduced in order to maintain a flow of power as opposed to stopping the blades entirely.

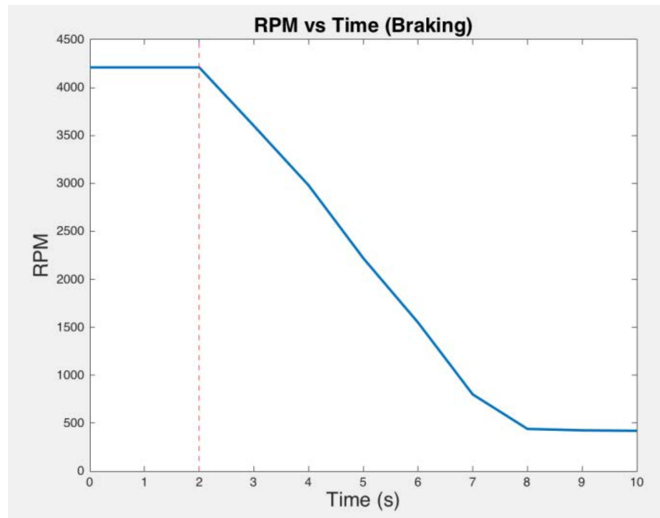

Figure 29: RPM vs. Time (Braking)

Testing Objective 5 – Assessment of the Yaw System

Because the wind tunnel did not have an actively controlled turntable, the yaw capabilities of the turbine were assessed through an initial perturbation. The turbine was forcibly yawed to an initial angle, and then released. The time to reach a steady state yaw angle of 0 degrees was then measured. The chart above quantifies the time to steady state. It is interesting to note that the time to steady state decreased with increasing perturbation angle. This is because the restoring moment increases with the perturbation angle, causing the initial acceleration to be large as the turbine moves back to steady state.

Test Wind Speed (m/s)	**Approximate Yaw Angle** (degrees)	**Time to Steady State** (seconds)
6.75	30°	5.14
	45°	3.61
	70°	2.62
9.15	20°	3.24
	30°	2.66
	45°	1.84
16.0	18°	1.16
	25°	1.05
	33°	0.97

Figure 30: Yaw Analysis

Appendix: Engineering Drawings

Note: All dimensions in inches

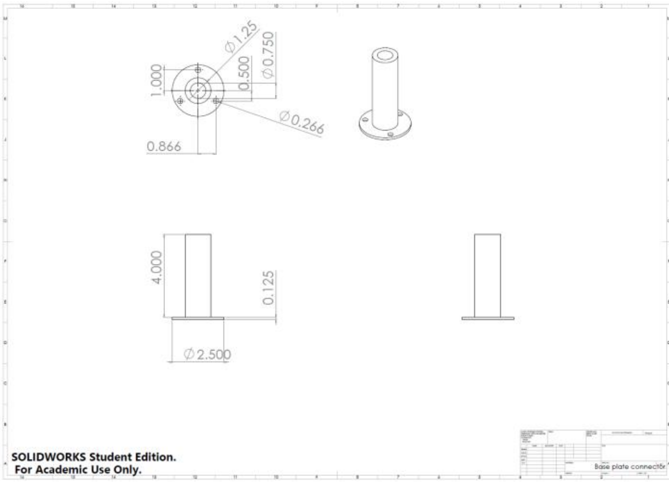

Appendix A: Base Plate Connector

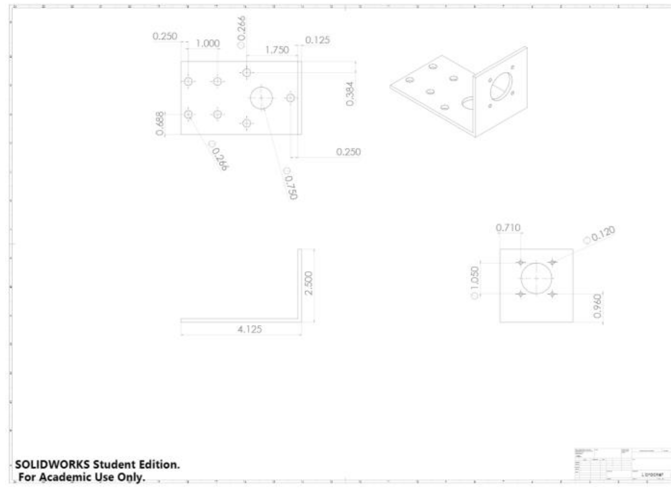

Appendix B: L Bracket

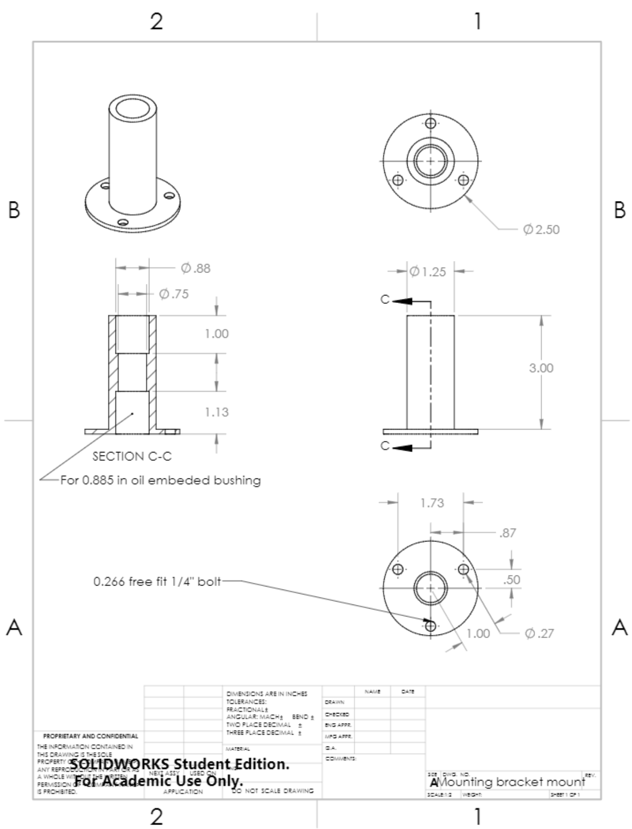

Appendix C: Mounting Bracket

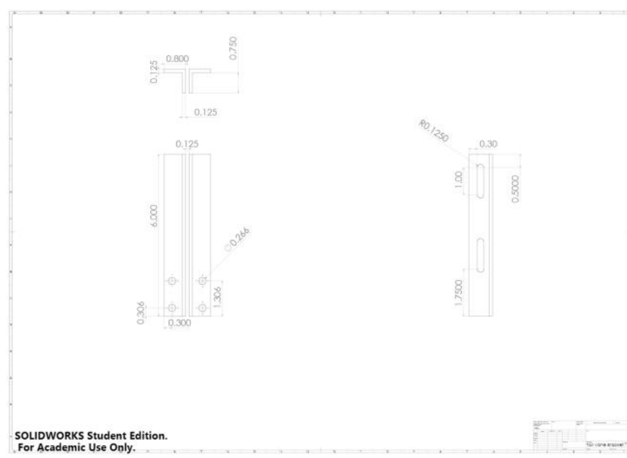

Appendix D: Tale Vane Mount

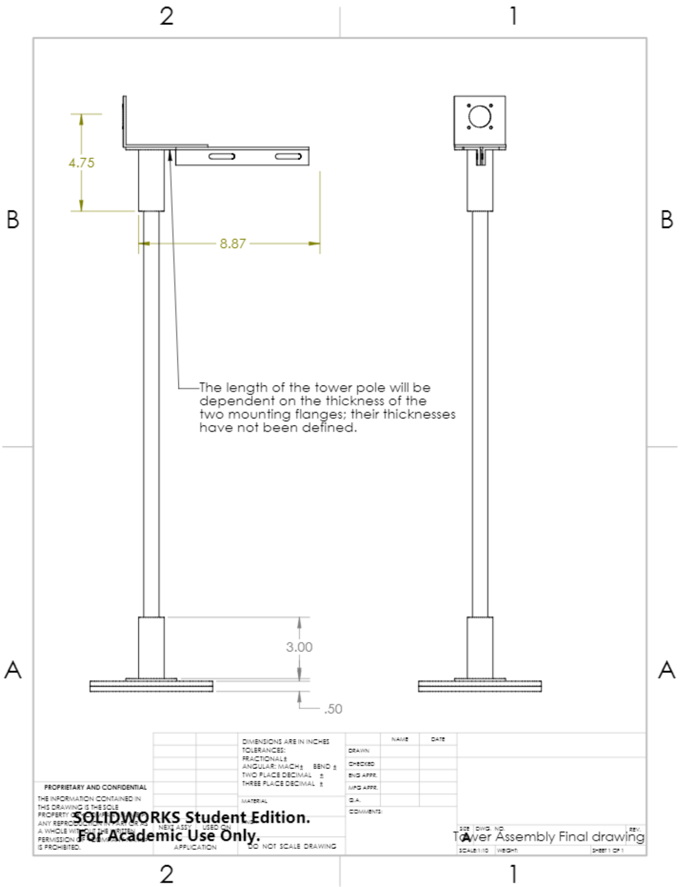

Appendix E: Tower Assembly

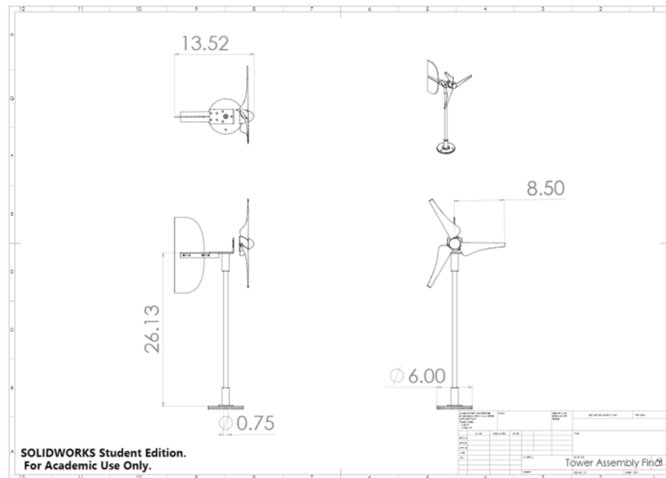

Appendix F: Tower Assembly

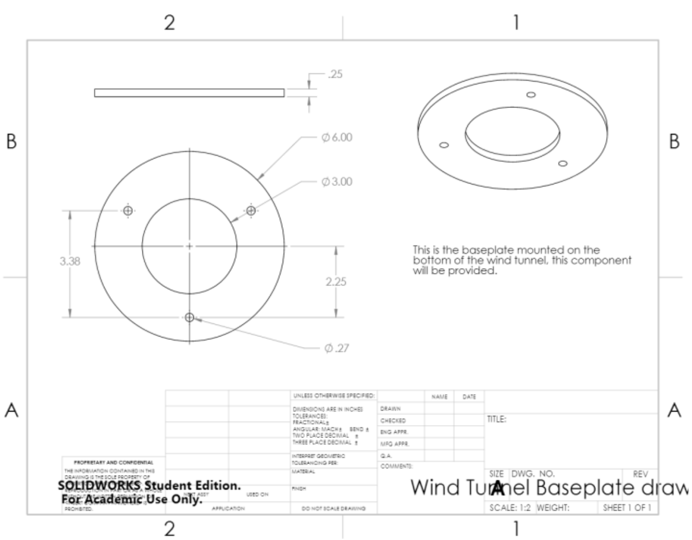

Appendix G: Baseplate

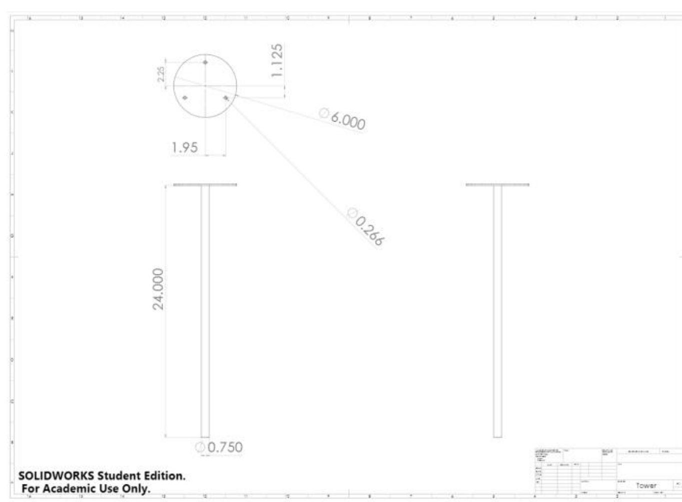

Appendix H: Tower